Supplementary Information

Core/shell Template-derived Co, N-doped Carbon Bifunctional Electrocatalysts for Rechargeable Zn-air Battery

Yanlong Lv[1], Lin Zhu[1], Haoxiang Xu[1], Liu Yang[1], Zhiping Liu[1,*], Daojian Cheng[1], Xiaohua Cao[2], Jimmy Yun[3], Dapeng Cao[1, 2, *]

[1] State Key Laboratory of Organic-Inorganic Composites and Beijing Advanced Innovation Center for Soft Matter Science and Engineering, Beijing University of Chemical Technology, Beijing 100029, People's Republic of China

[2] College of Chemical and Environmental Engineering, Jiujiang University, Jiujiang, Jiangxi 332005, P. R. China

[3] School of Chemical Science and Engineering, The University of New South Wales, Sydney, NSW 2052, Australia

* Corresponding Author. Email: liuzhp@mail.buct.edu.cn or caodp@mail.buct.edu.cn

Section S1. Experimental

S1.1 Synthesis of Carbon-Z1

The ZnO@ZIF-67 particles are dispersed in a ceramic boat, heated to 300 ℃ and maintained for 2h in a tube furnace. The temperature in the furnace is further raised to 950℃ at a ramp rate of 4℃·min^{-1} and kept at that temperature for 2 h. After that, the furnace is cooled down to room temperature naturally. During the pyrolysis process, the furnace is under Ar flow. The as-prepared black powder products are collected with no further operation.

S1.2 Synthesis of Carbon-2

$Co(NO_3)_2$ $6H_2O$ (0.2g) and melamine/glucose (1g/1g) are dispersed in a solution of 150ml methanol. The mixture was kept at room temperature for 12h under continuous stirring. The precipitate is collected by filtration, washed with methanol for several times and dried at 60 ℃ (~12h). The as-prepared powder is dispersed in a ceramic boat, heated to 300 ℃ and maintained for 2 h in a tube furnace. The temperature in the furnace is further raised to 950 ℃ at a ramp rate of 4 ℃·min^{-1} and kept at that temperature for 2h. After that, the furnace is cooled down to room temperature naturally. During the pyrolysis process, the furnace is under Ar flow. The as-prepared black powder products are collected with no further operation.

S1.3 Synthesis of Carbon-3

ZnO (0.2g) and melamine/glucose (1g/1g) are dispersed in a solution of 150ml methanol. The mixture was kept at room temperature for 12h under continuous stirring. The precipitate is collected by filtration, washed with methanol for several times and dried at 60 ℃ (~12h). The as-prepared powder is dispersed in a ceramic boat, heated to 300 ℃ and maintained for 2 h in a tube furnace. The temperature in the furnace is raised to 850 ℃ at a ramp rate of 4 ℃·min^{-1} and kept at that temperature for 1 h. After that, the furnace is cooled down to room temperature naturally. During the pyrolysis process, the furnace is under Ar flow. The as-prepared black powder products are collected with no further operation.

S1.4 Synthesis of Carbon-4

ZnO (0.1g) and ZIF-67 NPs (1g) are grinded for about 0.5 h in a mortar. After grinding treatment,

the as-prepared powder is put into a ceramic boat, heated to 300 ℃ and maintained for 2 h in a tube furnace. The temperature in the furnace is raised to 950 ℃ at a ramp rate of 4 ℃·min $^{-1}$ and kept at that temperature for 2 h. After that, the furnace is cooled down to room temperature naturally. During the pyrolysis process, the furnace is under Ar flow. The as-prepared black powder products are collected with no further operation.

S1.5 Structure characterization

The PXRD measurements were performed with a D8 ADVANCE X-ray diffractometer (Cu-Kα, 40 kV, 20 mA, λ =1.54178 Å). Scanning electron microscopy (SEM) images were obtained with a Cambridge S250MK3 SEM instrument. High-resolution transmission electron microscopy (HRTEM) was performed with a JEOL JEM-7001F and a JEOL JEM-ARM200F instrument. The thermogravimetric analysis (TGA) data were obtained with a DTG-60A (SHIMADZU) instrument at a heating rate of 10 °C•min^{-1} under flowing N_2. Raman spectra were recorded with a LabRAM Aramis Raman Spectrometer (HORIBA Jobin Yvon). The XPS data was recorded with a ThermoFisher ESCALAB 250 X-ray photoelectron spectrometer equipped with a twin anode Mg-Kα X-ray source. The cobalt K-edge spectra were collected at the Beijing Synchrotron Radiation Facility, (BSRF) China, on beamline 4W1B with an electron energy of 2.5 GeV and a maximum current of 250 mA. The intensity of the incident X-ray was monitored by an N_2-filled ion chamber (I_0) in front of the sample. N_2 adsorption/desorption isotherms at 77 K were measured by a Micromeritics ASAP 2020. ICP spectroscopy was performed with a Thermo 6300 spectrometer.

S1.6 Electrochemical characterization

A rotating disk electrode (RDE, RRDE-3A, BAS Inc.) with glassy carbon disk electrode (GC, 5 mm in diameter) and a rotating ring-disk electrode (RRDE, UJ126) with a GC disk (4 mm in diameter) and a Pt ring (5 mm inner diameter and 7 mm outer diameter) were polished with a 0.5, 0.15, and 0.05μm alumina slurry in turn and subsequently rinsed with ultrapure water and ethanol. To prepare the working electrode, the carbon catalyst (5 mg) was dispersed ultrasonically in a mixture of 2-propanol (400μL), deionized water (600μL), and 0.5% Nafion (10μL), and the resulting catalyst ink (10μL) was dropped onto the GC surface and dried at room temperature. For comparison, a commercial Pt/C catalyst (20% Pt/C) was prepared using the same method. To evaluate the ORR activity, the

electrochemical measurements, including CV, rotating disk electrode (RDE) measurements, rotating ring-disk electrode (RRDE) measurements, and chronoamperometry were performed at room temperature in 0.1 M KOH solutions. Particularly, linear sweep voltammograms (LSV) for the OER were obtained using a RDE in 1 M KOH solution, corrected by iR-compensation. All the electrochemical tests were performed in a standard three electrode cell with a Pt net as the counter electrode and Ag/AgCl (saturated KCl) reference electrode. The electrochemical properties were investigated by CV and LSV with a CHI760e instrument from CH Instruments Inc. Before the measurements, the electrolyte was saturated with oxygen/nitrogen through bubbling.

S1.7 Calculation of electron transfer number (n) and hydrogen peroxide yield

Koutecky-Levich plots were analyzed at various electrode potentials. The number of electrons transferred (n) were calculated by the slopes of the linear fitting on the basis of the following Koutecky-Levich equations

$$\frac{1}{J}=\frac{1}{J_l}+\frac{1}{J_k}=\frac{1}{B\omega^{1/2}}+\frac{1}{J_k} \tag{S1}$$

$$J_k = nF\kappa C_0 \tag{S2}$$

$$B = 0.2nFC_0(D_0)^{2/3}\nu^{-1/6} \tag{S3}$$

where J is the measured current density, J_k and J_l are the kinetic- and diffusion-limiting current densities, ω is the angular velocity of the disk (ω=2πN, N is the linear rotation speed), n is the overall number of electrons transferred in oxygen reduction reaction, F is the Faraday constant (F=96485 C mol^{-1}), κ is the electron-transfer rate constant, C_0 is the bulk concentration of O_2, and υ is the kinematic viscosity of the electrolyte. In 0.1 M KOH, the values can be determined: C_0= 1.2×10^{-3} mol L^{-1}; D_0=1.9×10^{-5} cm s^{-1}; ν=0.1 m^2 s^{-1}.

The electron transfer number per O_2 and $\%HO_2^-$ were calculated from the RRDE measurement.

$$n = 4I_d/\left(I_d + I_r/N\right) \tag{S4}$$

$$\%HO_2^- = 200\times\frac{I_r/N}{I_d + I_r/N} \tag{S5}$$

Here I_d is the disk current, I_r is the ring current and N is the current collection efficiency of Pt ring (N=0.42).

S1.8 Fabrication of a Zn-air battery

The Zn-air batteries were tested in home-built electrochemical cells using a zinc plate as the anode and a carbon cloth as the air cathode. The catalysts loading on carbon cloth are 1 mg cm^{-2} of Pt/C and 1mg cm^{-2} of IrO_2 for Pt-IrO_2 battery and 1 mg cm^{-2} of Carbon-ZNC for Carbon-ZNC battery. The electrolyte used is 6.0 M KOH with 0.2 M zinc acetate to ensure reversible Zn electrochemical reactions at the anode. Measurements were carried out at room temperature with a LAND CT2001A multi-channel battery testing system.

Section S2. Theoretical Calculations

S2.1 Electrochemical framework

The ORR activities on various electrocatalysts were studied in detail according to electrochemical framework developed by Nørskov and his co-workers [1-3]. We have considered the overall ORR process in alkaline conditions. As for ORR, O_2 is reduced either through a two-electron process, or completely via a direct four-electron pathway. Here, we only focus on four-electron reduction of O_2 because previous results showed that the ORR proceeds on doped graphene through the complete reduction cycle[4, 5].

In an alkaline electrolyte (pH=14), H_2O rather than H_3O^+ may act as the proton donor, so overall reaction scheme of the oxygen reduction reaction (ORR) and oxygen evolution reaction (OER) can be written as:

$$\mathbf{O_2 + 2H_2O + 4e^- \leftrightarrow 4OH^-}$$

S2.2 Reaction free energy

The theoretical on-set potentials and overpotentials of the ORR/OER processes can be determined by examining the reaction free energies of the different elementary steps. The free energy diagram is established by considering the binding of reactants, the various intermediates and final products of reaction. The Gibbs reaction free energy of these electrochemical elementary steps involving electron/proton transfer was obtained by using density functional theory (DFT) calculations accompanied with computational normal hydrogen electrode (NHE) model developed by Nørskov and

co-workers[1, 3, 7]. In this model, the calculation of reaction free energy is performed by setting up NHE as the reference electrode, which allows us to replace chemical potential for ($H^+ + e^-$) with that of half a hydrogen molecule at standard conditions (U = 0 V vs NHE, pH=0, p = 1 bar, T = 298 K).

In order to obtain the reaction free energy of each elementary step in ORR/OER on different sites for various model electrocatalysts, we calculated the adsorption free energy of O^*, OH^* and OOH^*. Since it is difficult to obtain the exact free energy of OOH, O, and OH radicals in the electrolyte solution, the adsorption free energy ΔG_{OOH*}, ΔG_{O*}, and ΔG_{OH*}, are relative to the free energy of stoichiometrically appropriate amounts of H_2O (g) and H_2 (g) [8]. The relevant data are shown in Table S4.

For each elementary step, the Gibbs reaction free energy ΔG is defined as the difference between free energies of the initial and final states and is given by the expression:

$$\Delta G = \Delta E + \Delta ZPE - T\Delta S + \Delta G_U + \Delta G_{PH}$$

where ΔE is the reaction energy of reactant and product molecules adsorbed on catalyst surface, obtained from DFT calculations; ΔZPE and ΔS are the change in zero point energies and entropy due to the reaction.

For our co-supported and freestanding graphene and pdN-graphene system, the reaction free energy for ORR can be expressed with the adsorption free energy of various oxygenated species, gas phase H_2 and H_2O defined earlier, which are

$$\Delta G_1 = \Delta G_O^* - 4.92 + eU + pH \times k_B T \ln 10 \quad \text{(S6)}$$

$$\Delta G_2 = \Delta G_O^* - \Delta G_{OOH}^* + eU + pH \times k_B T \ln 10 \quad \text{(S7)}$$

$$\Delta G_2 = \Delta G_{OH}^* - \Delta G_O^* + eU + pH \times k_B T \ln 10 \quad \text{(S8)}$$

$$\Delta G_3 = -\Delta G_{OH}^* + eU + pH \times k_B T \ln 10 \quad \text{(S9)}$$

The reaction free energy of reaction S11−S13 for OER can be calculated using the following equations:

$$\Delta G_4 = \Delta G_{OH}^* - eU - pH \times k_B T \ln 10 \quad \text{(S10)}$$

$$\Delta G_7 = \Delta G_{OOH}^* - \Delta G_O^* - eU - pH \times k_B T \ln 10 \quad \text{(S11)}$$

$$\Delta G_5 = \Delta G_O^* - \Delta G_{OH}^* - eU - pH \times k_B T \ln 10 \quad \text{(S12)}$$

$$\Delta G_6 = 4.92 - \Delta G_O^* - eU - pH \times k_B T \ln 10 \quad \text{(S13)}$$

S2.4 Free energy diagram, on-set potential and overpotential

The elementary step which has the highest value for ΔG at the standard equilibrium potential from the free energy diagram has been termed the potential-determining step[9]. It is the last step to become downhill in free energy as the potential increased to on-set potential, which represents the thermodynamically least favorable reaction step in the ORR/OER on the electrocatalyst surface. Nørskov *et al*. developed a definition for overpotentials[1, 2]. An applied potential U is required to overcome the positive free energy change of potential-determining step, determining overpotential:

$$G^{ORR} = (\Delta G_1, \Delta G_2, \Delta G_3, \Delta G_4)$$

$$\eta^{ORR} = 1.23 + G^{ORR}\ \mathrm{V} \qquad \text{(S12)}$$

$$G^{OER} = (\Delta G_5, \Delta G_6, \Delta G_7, \Delta G_8)$$

$$\eta^{OER} = 1.23 - G^{OER}\ \mathrm{V} \qquad \text{(S13)}$$

ΔG_1~ ΔG_6 are the free energy of Reactions (S6)-(S11) on the RHE scale, respectively.

The free energy diagram for the ideal (but nonexistent) ORR/OER catalyst is shown in Figure S17a and c. In order to facilitate O_2 reduction at the equilibrium potential, reaction free energies of all the four proton-transfer steps should be the same (1.608 V/4=0.402 V vs NHE) at zero potential at ideal catalyst, in other words, all the reaction free energies require to be zero at the equilibrium potential, 0.402 V. The material which has this behavior is regarded as thermochemically ideal bifuntional ORR/OER electrocatalyst. Real catalysts including the outstanding catalysts predicted theoretically for ORR, like Pt, do not fulfill this requirement. The calculated free energy diagrams at standard conditions of the ORR on the Pt (111) surfaces are shown in Figure S17b, with the same computational detail and models as reference[1]. It's observed that all the elementary steps are slightly uphill except the second step in terms of ΔG_1~ ΔG_4 at U = 0. At the standard equilibrium potential, U^0_{NHE}, all steps become more uphill with more positive ΔG except that the second step is still downhill since the intermediate stage (O^*) is too stable as well as OH^*. The onset potential for a downhill reduction process is found to be $U^{on\text{-}set}_{NHE}$ = -0.024 V, corresponding to an overpotential of η = -0.42 V. Real catalysts including the outstanding catalysts predicted theoretically for OER, like IrO_2, do not fulfill ideal requirement either. The corresponding free energy diagram is shown in Figure S17d, with the same computational detail and models as reference[2]. We observe that at U = 0 V, all the elementary steps except the first step are uphill according to ΔG_5~ ΔG_8. At the equilibrium potential of U^0 = 0.402 V, the first intermediates (OH^*) have negative ΔG, and other steps remain uphill, as mentioned above. We observe that the lowest working potential, or onset potential, for a downhill water oxidation process is $U^{on\text{-}set}_{NHE}$ = 1.052 V,

corresponding to an overpotential of η = -0.65 V.

References

1. Nørskov, J. K.; Rossmeisl, J.; Logadottir, A.; Lindqvist, L.; Kitchin, J. R.; Bligaard, T.; Jónsson, H. Origin of the Overpotential for Oxygen Reduction at a Fuel-Cell Cathode. *J. Phys. Chem. B* 2004, 108, 17886-17892.
2. Man, I. C.; Su, H. Y.; Calle-Vallejo, F.; Hansen, H. A.; Martínez, J. I.; Inoglu, N. G.; Kitchin, J.; Jaramillo, T. F.; Nørskov, J. K.; Rossmeisl, J. Universality in Oxygen Evolution Electrocatalysis on Oxide Surfaces. *ChemCatChem* 2011, 3, 1159-1165.
3. Rossmeisl, J.; Qu, Z. W.; Zhu, H.; Kroes, G. J.; Nørskov, J. K. Electrolysis of Water on Oxide Surfaces. *J. Electroanal. Chem.* 2007, 607, 83-89.
4. Jiao, Y.; Zheng, Y.; Jaroniec, M.; Qiao, S. Z. Origin of the Electrocatalytic Oxygen Reduction Activity of Graphene-Based Catalysts: A Roadmap to Achieve the Best Performance. *J. Am. Chem. Soc.* 2014, 136, 4394-4403.
5. Zhang, L.; Xia, Z. Mechanisms of Oxygen Reduction Reaction on Nitrogen-Doped Graphene for Fuel Cells. *J. Phys. Chem. C* 2011, 115, 11170-11176.
6. Desai, S. K.; Neurock, M. First-principles Study of the Role of Solvent in the Dissociation of Water over a Pt-Ru Alloy. *Phys. Rev. B* 2003, 68, 1071-1086.
7. Rossmeisl, J.; Logadottir, A.; Nørskov, J. K. Electrolysis of Water on (Oxidized) Metal Surfaces. *Chem. Phys.* 2005, 319, 178-184.
8. Atkins, P. W.; De Paula, J. *Physical Chemistry, 9th ed.* Oxford University Press: Oxford, U.K., 2010; p 472, 922, 924, 933.
9. Koper; Marc, T. M. Thermodynamic Theory of Multi-electron Transfer Reactions: Implications for Electrocatalysis. *J. Electroanal. Chem.* 2011, 660, 254-260.

Table S1. Surface species concentration for Cabon-Z1 and Carbon-ZNC summarized by XPS results[a]

samples	C	N	O	Co
Carbon-Z1	76.08	2.13	15.42	6.37
Carbon-ZNC	84.25	1.61	13.28	0.86

[a] Hydrogen is not taken into account for the calculation

Table S2. EXAFS fitting parameters at the Co K-edge for various samples

samples	shell	N [a]	R (Å) [b]	σ^2 (Å^2 ·10^3) [c]	ΔE_0 (eV) [d]	R factor (%)
Carbon-ZNC	Co-N	0.7	1.93	5.1	8.1	0.2
	Co-Co	10.6	2.50	6.4	7.6	
Carbon-Z1	Co-Co	11.6	2.49	6.4	7.3	0.1
Co-foil	Co-Co	12	2.49	6.7	7.2	0.1

[a] N: coordination numbers; [b] R: bond distance; [c] σ^2: Debye-Waller factors; [d] ΔE_0: the inner potential correction. R factor: goodness of fit. $S0^2$ for Co-Co is 0.80, For Co-N is 0.80, were obtained from the experimental EXAFS fit of Co foil references by fixing CN as the known crystallographic value and was fixed to all the samples.

Table S3. Summary of porosity parameters of Carbon-Z1 and Carbon-ZNC

samples	S_{BET}[a] (m^2g^{-1})	S_{Lamuir}(m^2g^{-1})	V_t[b](cm^3g^{-1})	V_{micro}[c](cm^3g^{-1})	V_{micro}/V_t(%)
Carbon-Z1	72	116	0.215	0.014	6.5
Carbon-ZNC	230	353	0.41	0.10	24.4

[a] The specific surface area was calculated by the Brunauer-Emmett-Teller (S_{BET}) method. S_{BET} calculated in the region of P/P_0 =0.05 to 0.3. [b] V_t represents the total pore volume, determined at P/P0=0.9997. [c] V_{micro} represents the volume of micropore.

Table S4. Values used for the entropy and zero-point energy corrections in determining the free energy of reactants, products, and intermediate species adsorbed on clusters. For the surface bound species, the ZPE values are averaged over model structures

Species	T×S (eV) (298K)	ZPE (eV)
O*	0	0.07
OH*	0	0.33
OOH*	0	0.43
H_2(g)	0.41	0.27
H_2O(g)	0.58	0.57

Table S5. Adsorption free energies of OH, O and OOH (eV) on the most active sites on catalysts

	ΔG^*_{OH}	ΔG^*_O
Pt(111)	0.80	1.62
IrO_2(110)	0.11	1.36
pdN	0.20	0.91
pdN-Co	3.32	3.46

Table S6. Reaction free energy (eV vs RHE) of elementary step for ORR/OER at U=0, pH=14 on different active sites on catalysts

	ORR				OER			
	ΔG_1	ΔG_2	ΔG_3	ΔG_4	ΔG_5	ΔG_6	ΔG_7	ΔG_8
Pt(111)	-0.82	-2.97	-0.82	-0.80	0.80	0.82	2.97	0.82
IrO_2(110)	-1.68	-1.88	-1.25	-0.11	0.11	1.25	1.88	1.68
pdN	-4.23	*	-0.93	0.24	0.24	0.93	*	4.23
pdN-Co	-1.47	*	-0.56	-2.09	2.09	0.56	*	1.47

Table S7. Reaction On-set electron potential ($U^{on\text{-}set}$, V vs RHE), overpotential (η, V) for ORR and OER on different active sites on catalysts

	$U_{ORR}^{on\text{-}set}$	η_{ORR}	$U_{OER}^{on\text{-}set}$	η_{OER}
Pt(111)	-0.80	-0.42	2.48	-1.25
IrO_2(110)	-0.11	-1.12	1.88	-0.65
pdN	0.24	1.47	4.23	3.00
pdN-Co	0.56	0.67	2.89	1.66

Table S8. Comparison of the non-noble metal ORR catalysts from literature and this work

catalyst	electrolyte	E_{onset} vs. RHE (V)	$E_{1/2}$ vs. RHE(V)	Ref.
Co_3O_4/N-rmGO	0.1 M KOH	0.92	0.83	
ZIF-67-900	0.1 M KOH	0.91	0.85	
NC900 (ZIF-8)	0.1 M KOH	0.83	0.68	
Co@ Co_3O_4@C-CM	0.1 M KOH	0.93	0.81	
$NiCo_2O_4$	0.1 M KOH	0.80	0.74	
Co-N-C-800	0.1 M KOH	0.83	-	
Fe-N/C-800	0.1 M KOH	0.98	0.85	
PpPD-Fe-C	0.5 M H_2SO_4	0.83	-	
Carbon-ZNC	0.1 M KOH	0.91	0.81	this work

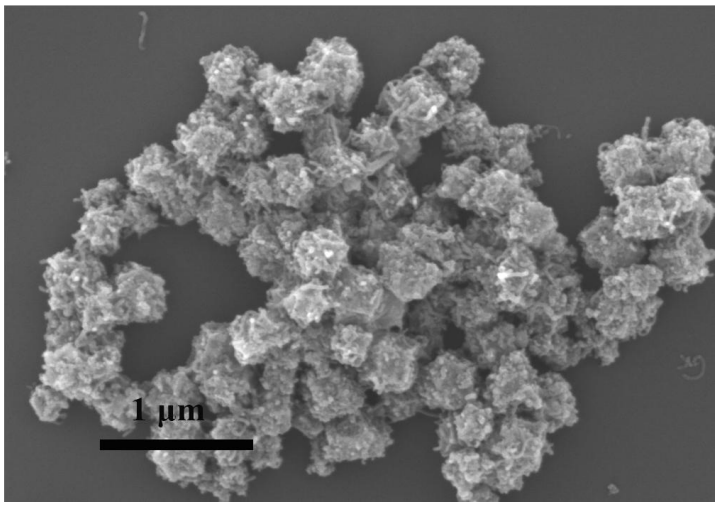

Figure S1. SEM image of Carbon-Z1.

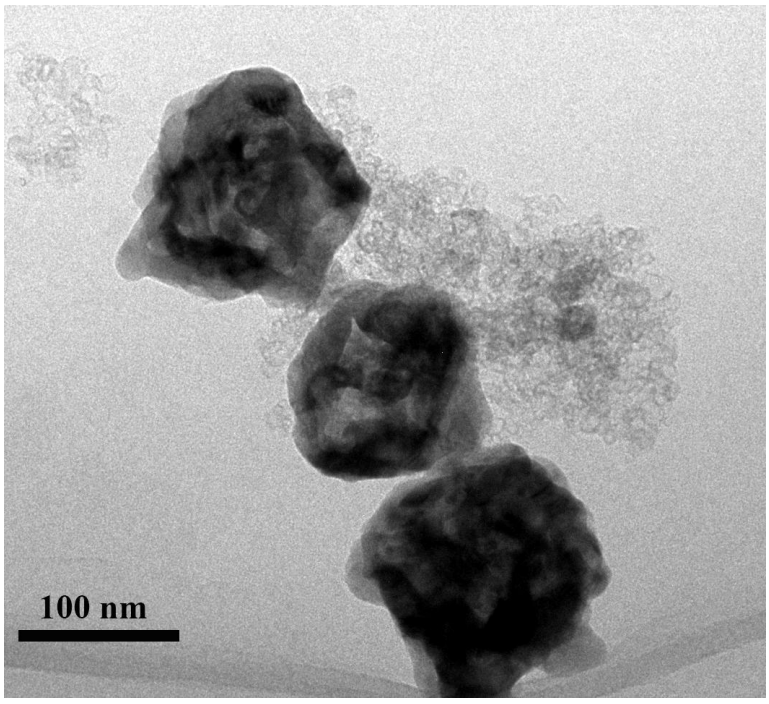

Figure S2. TEM image of Carbon-Z1.

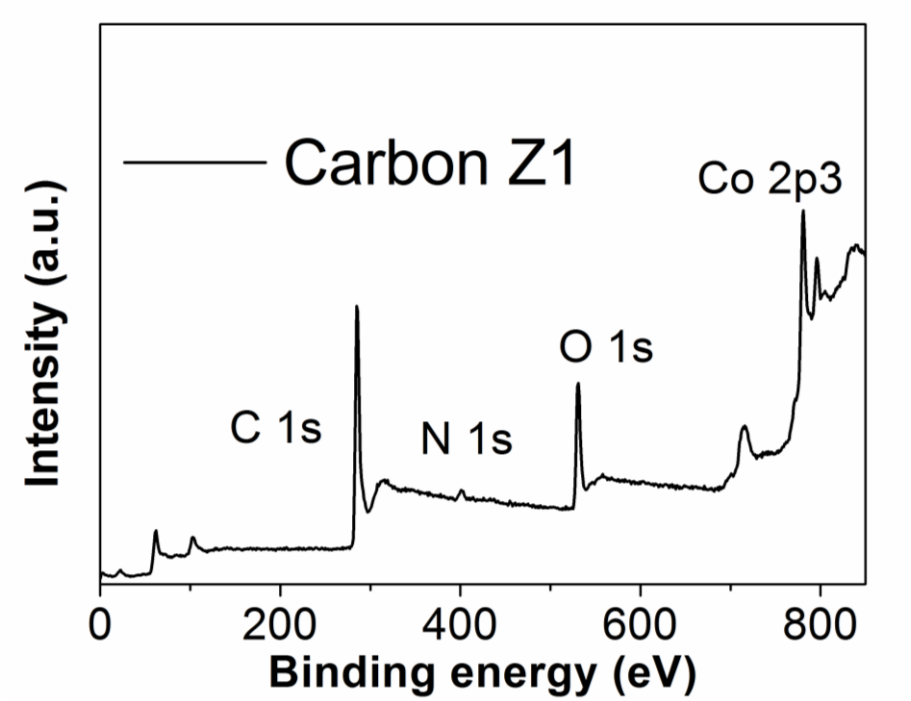

Figure S3. XPS spectra of Carbon-Z1.

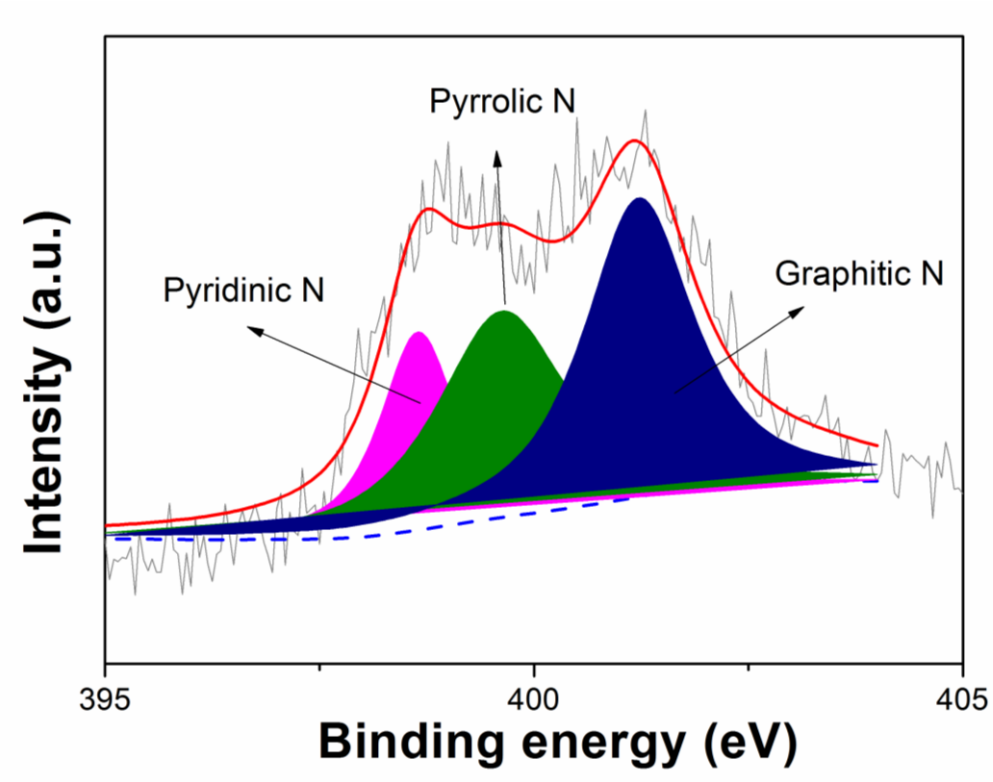

Figure S4. High–resolution N1s XPS spectra of Carbon-Z1.

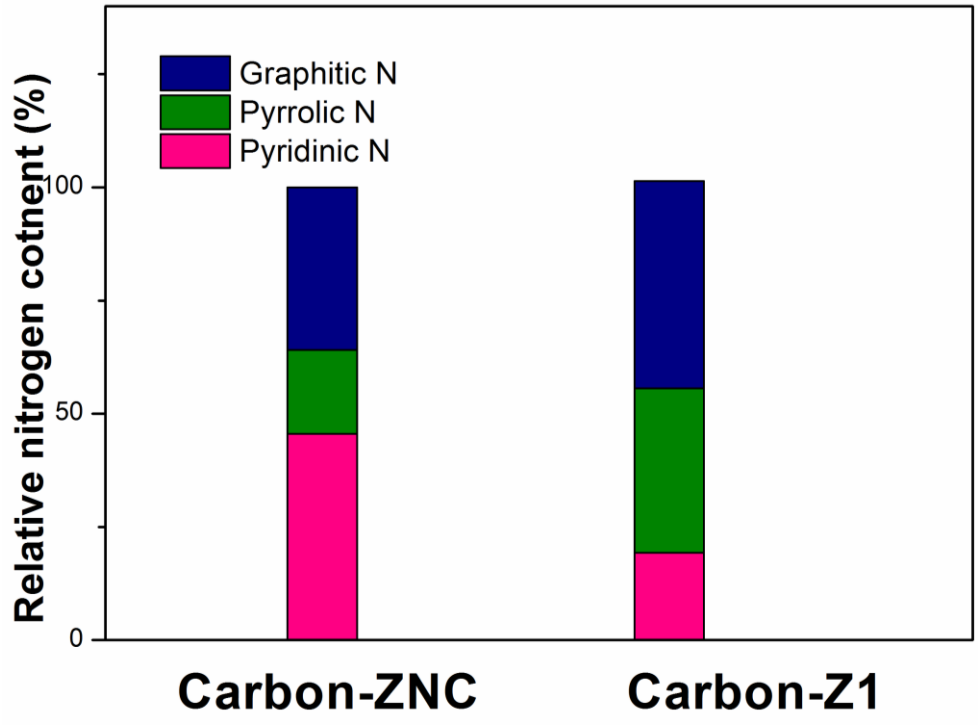

Figure S5. The relative content of three types of nitrogen in Carbon-ZNC and Carbon-Z1.

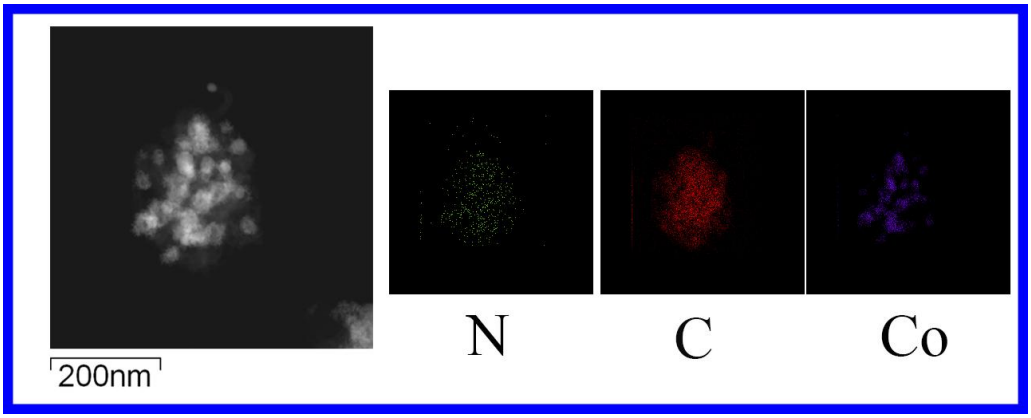

Figure S6. The TEM element mapping images of Carbon-ZNC (N, C and Co).

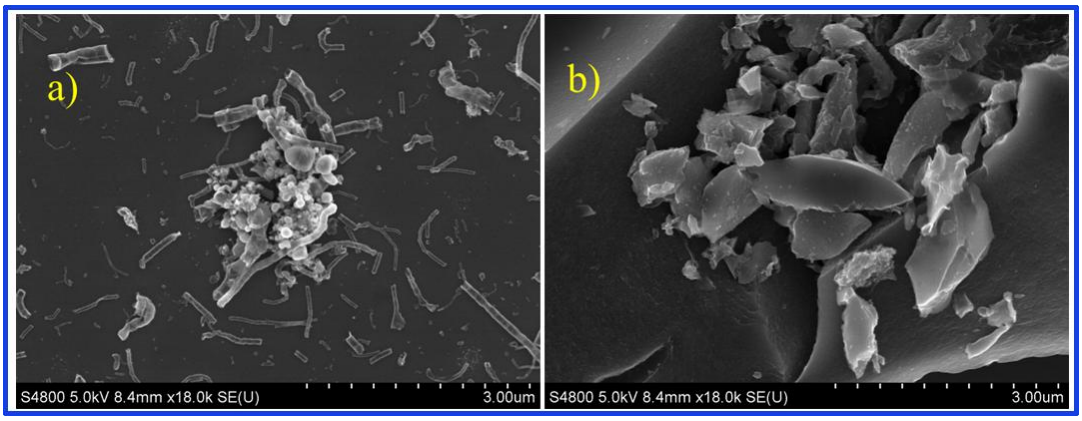

Figure S7. SEM images of as-prepared a) Carbon-2 and b) Carbon-3.

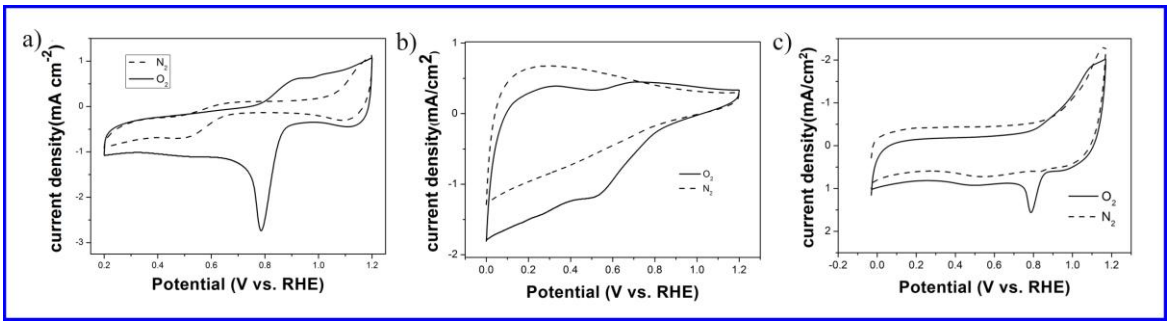

Figure S8. CV curves of a) Carbon-2, b) Carbon-3 and c) Carbon-4 in O_2-saturated (solid line) and N_2-saturated (dashed line) 0.1 M KOH with a sweep rate of 50 mV s^{-1}.

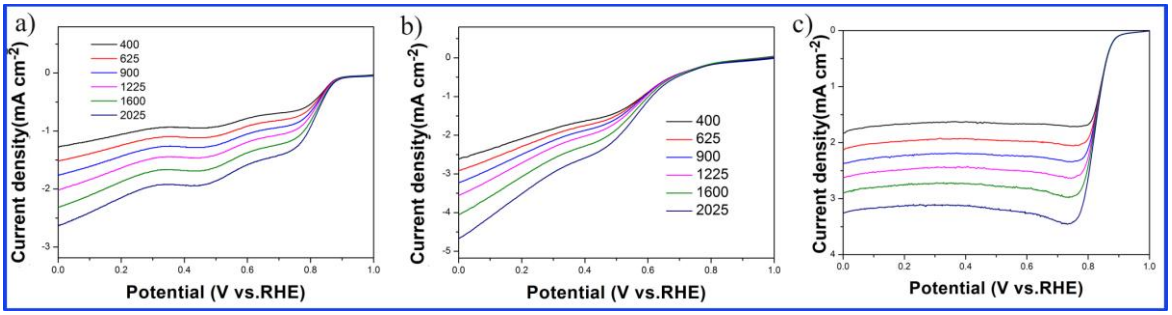

Figure S9. Rotating-disk voltammograms of a) Carbon-2, b) Carbon-3 and c) Carbon-4 in O_2-saturated 0.1 M KOH with a sweep rate of 5 mV s^{-1} at different rotation rates.

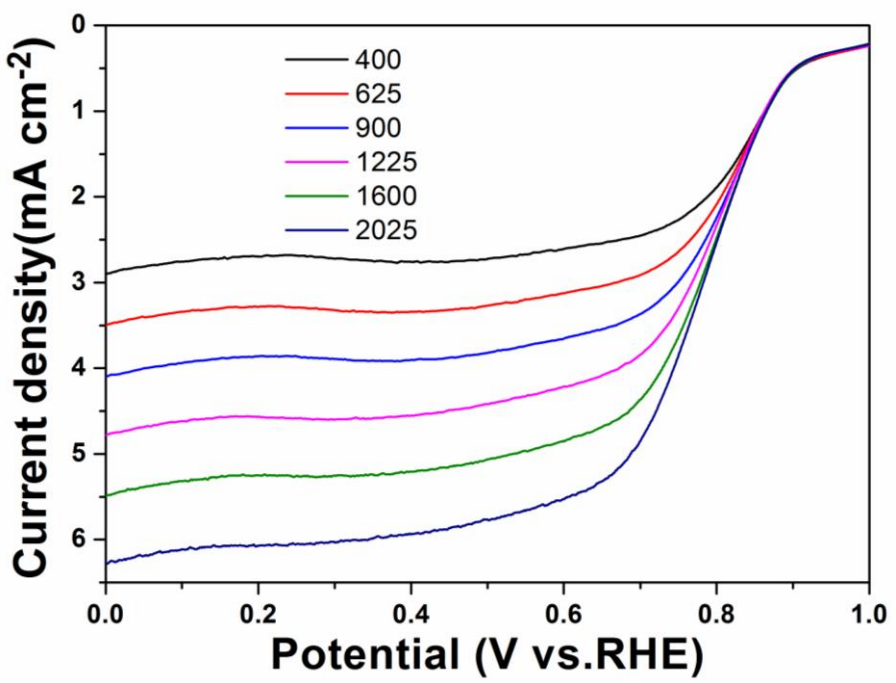

Figure S10. Rotating-disk voltammograms of Carbon-Z1 in O_2-saturated 0.1 M KOH with a sweep rate of 5 mV s^{-1} at different rotation rates.

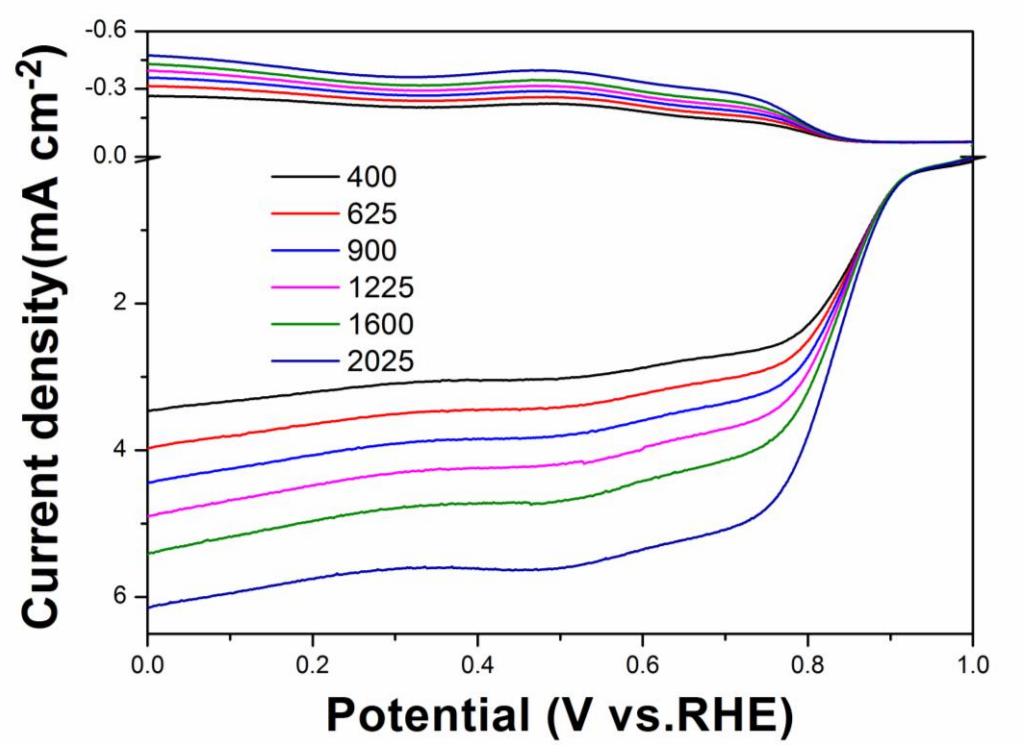

Figure S11. Rotating ring-risk electrode voltammograms of Carbon-Z1 in O_2-saturated 0.1M KOH recorded with different rotational speeds (from 400 to 2025 rmp).

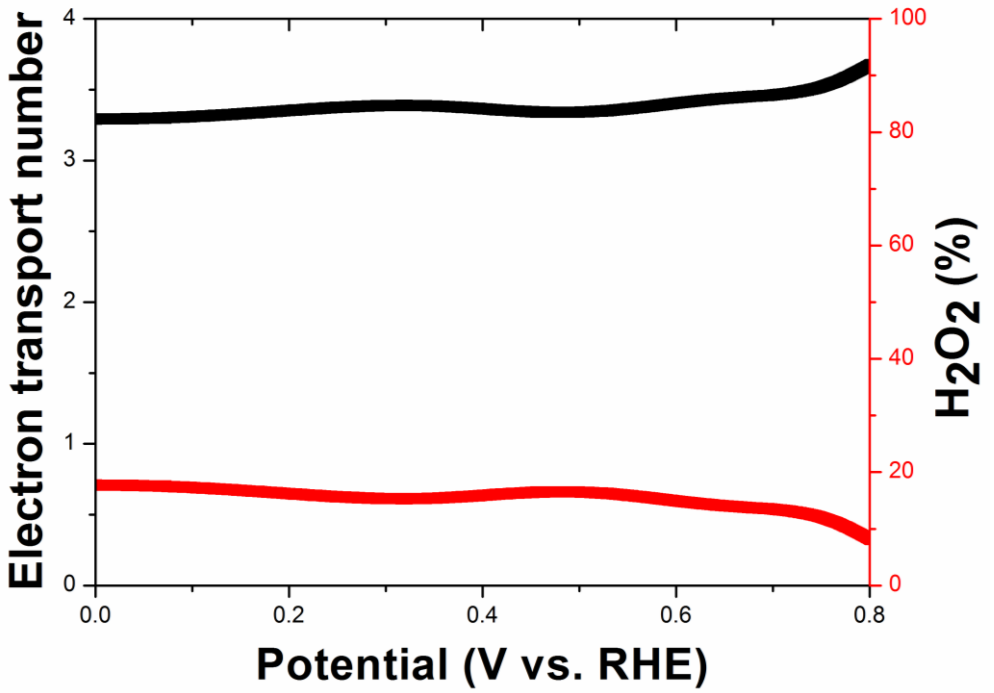

Figure S12. The electron number (n) and the production of hydrogen peroxide of Carbon-Z1 in the potential range of 0-0.8 V (vs. RHE).

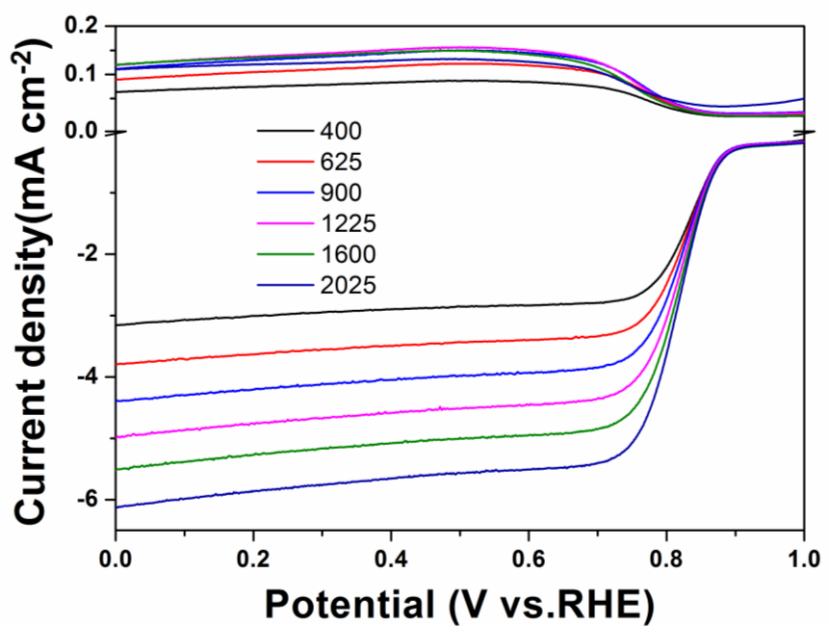

Figure S13. Rotating ring-risk electrode voltammograms of Carbon-ZNC in O_2-saturated 0.1M KOH recorded with different rotational speeds (from 400 to 2025 rmp).

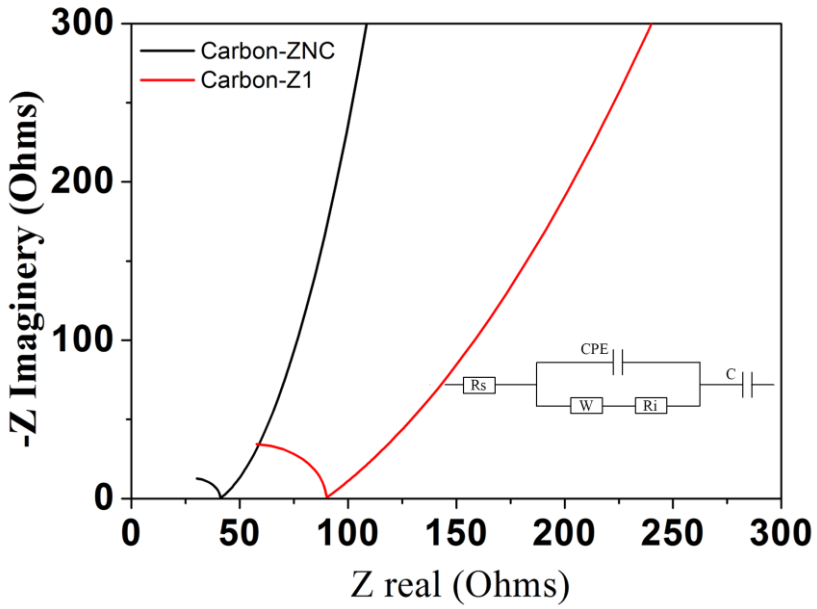

Figure S14. Nyquist spectra of Carbon-Z1 and Carbon-ZNC by applying a sine wave with amplitude of 5.0 mV over the frequency range from 100 kHz to 1 Hz in 0.1 M KOH.

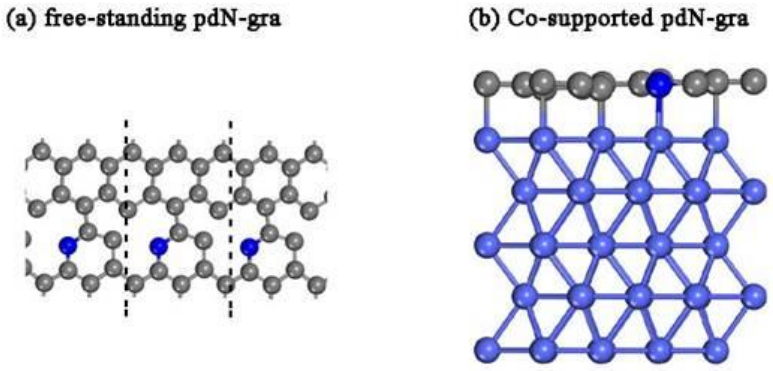

Figure S15. (a) pyridine N-dopedgraphene and (b) Co-supported pyridine N-doped graphene structures used in ourcalculation. Gray, blue and green balls represent C, N and Co atoms, respectively. PdN-gra is short for pyridine N-doped graphene.

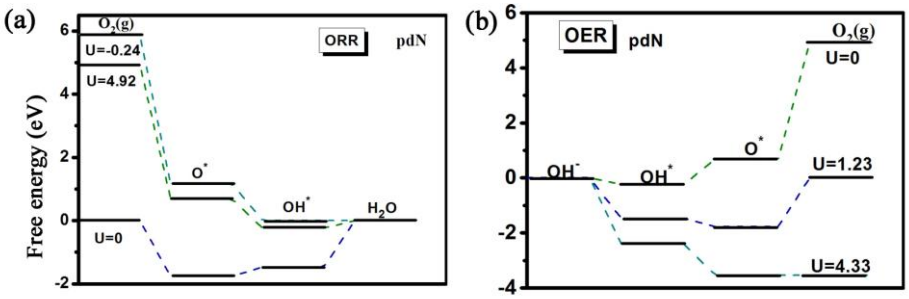

Figure S16. Free energy diagram for the ORR on (a) Co-supported pdN-doped graphene the OER on (b) Co-supported pdN-doped graphene surfaces.

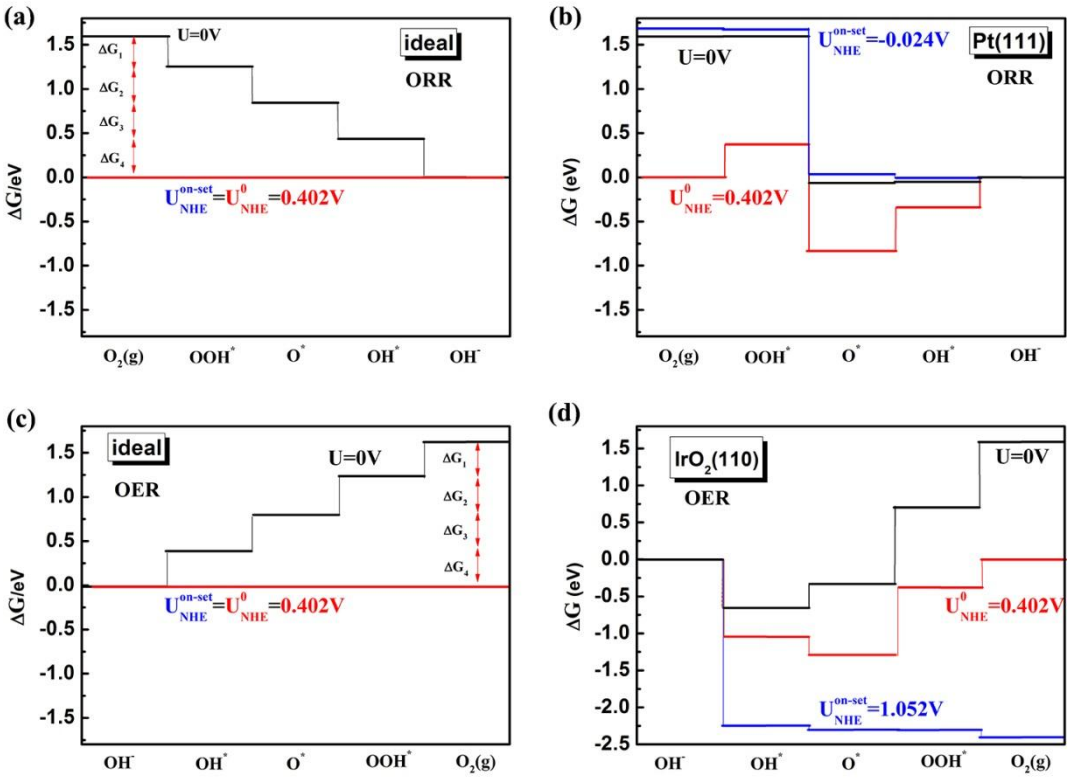

Figure S17. Free energy diagram for the ORR on (a) ideal catalyst and (b) Pt(111) surface, and the ORR on (c) ideal catalyst and IrO_2(110) at zero electrode potential, on-set electrode potential and equilibrium potential.

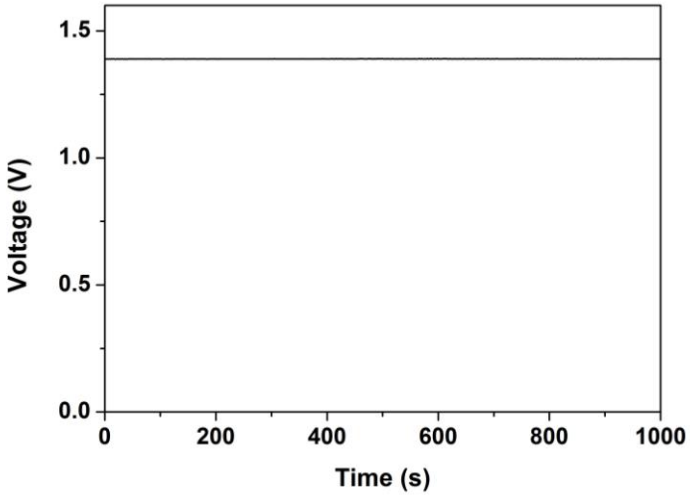

Figure S18. The open circuit plot of Carbon-ZNC battery

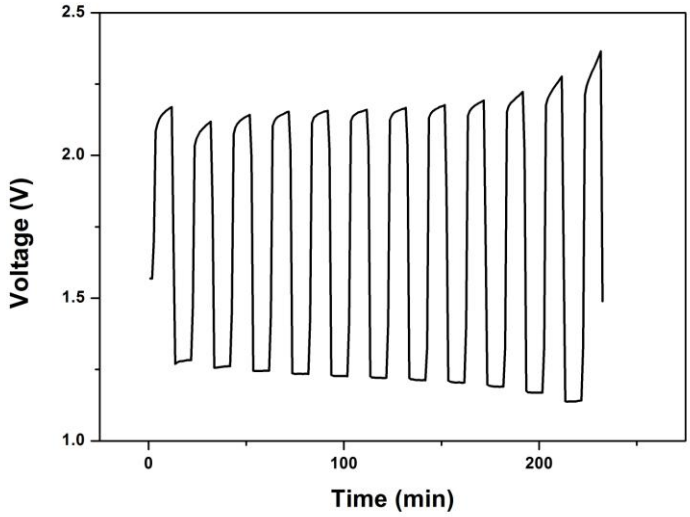

Figure S19. Cycling performance at the charging and discharging current density of Pt-IrO_2 at 5 mA cm^{-2}.